ELSEVIER

A kinetic mechanism for predicting secondary organic aerosol formation from toluene oxidation in the presence of NO_x and natural sunlight

Di Hu[a], Michael Tolocka[b], Qianfeng Li[a], Richard M. Kamens[a],*

[a]Department of Environmental Sciences and Engineering, the University of North Carolina at Chapel Hill, Chapel Hill, NC 27599, USA
[b]Department of Chemistry, Louisiana State University, Baton Rouge, LA 70803, USA

Abstract

A kinetic mechanism to predict secondary organic aerosol (SOA) formation from the photo-oxidation of toluene was developed. Aerosol phase chemistry that includes nucleation, gas–particle partitioning and particle-phase reactions as well as the gas-phase chemistry of toluene and its degradation products were represented. The mechanism was evaluated against experimental data obtained from the University of North Carolina (UNC) $270\,m^3$ dual outdoor aerosol smog chamber facility. The model adequately simulates the decay of toluene, the nitric oxide (NO) to nitrogen dioxide (NO_2) conversion and ozone formation. It also provides a reasonable prediction of SOA production under different conditions that range from 15 to $300\,\mu g\,m^{-3}$. Speciation of simulated aerosol material shows that up to 70% of the aerosol mass comes from oligomers and polymers depending on initial reactant concentrations. The dominant particle-phase species predicted by the mechanism are glyoxal oligomers, ketene oligomers from the photolysis of the toluene OH reaction product 2-methyl-2,4-hexadienedial, organic nitrates, methyl nitro-phenol analogues, C7 organic peroxides, acylperoxy nitrates and for the low-concentration experiments, unsaturated hydroxy nitro acids.
© 2007 Elsevier Ltd. All rights reserved.

Keywords: Toluene; Kinetic mechanism; Aerosol modeling; Secondary organic aerosol (SOA)

1. Introduction

Aromatic hydrocarbons are an important class of volatile organic compounds (VOCs) present in the atmosphere, and their yearly global emission concentrations are estimated to range from 18.7 to $25\,Tg\,yr^{-1}$ (Piccot et al., 1997; Ehhalt, 1999). Toluene is the most abundant of the aromatic hydrocarbons, and it has an average atmospheric concentration ranging from 50 ppt V in rural air to 10 ppb V or higher in urban air. Most atmospheric aromatics emissions come from anthropogenic sources such as transportation, solvent use and fuel combustion (Calvert et al., 2002). The major removal pathway of aromatic hydrocarbons from the atmosphere is through reaction with the hydroxyl radical (OH) (Calvert et al., 2002). Single ring aromatic hydrocarbons, because of their high anthropogenic emission and atmospheric rates, are significant contributors to ozone and secondary

*Corresponding author. Tel.: +1 919 966 5452;
fax: +1 919 966 7911.
E-mail address: kamens@unc.edu (R.M. Kamens).

organic aerosol (SOA) formation in urban areas (Makar et al., 2003). A model calculation predicts that up to 40% of photochemically produced ozone over northern Europe can be attributed to emissions of aromatics (Derwent et al., 1996). Highly oxygenated compounds, such as hydroxyaldehydes, polyketones and hydroxyketoacids formed during the photo-oxidation of toluene have been identified in many chamber studies (Edney et al., 2001; Jang and Kamens, 2001b; Kleindienst et al., 2004). These products have relatively low vapor pressures that can either self-nucleate to form ultra fine particles or rapidly partition onto existing particles and reach a gas–particle equilibrium (Holes et al., 1995; Odum et al., 1997; Jang and Kamens, 2001b; Hurley et al., 2001). However, recent product studies on the identification of toluene SOA by Hamilton et al. (2005) suggest that these C3–C7 oxygenated products contribute no more than 10% of the toluene SOA mass.

In addition to gas–particle partitioning, heterogeneous reactions are proposed to take place in the particle phase. This aids in the reactive uptake of volatile aldehyde compounds and the formation of large molecules within the aerosol. Oligomers formed by particle-phase reactions have been observed in the α-pinene system in the presence of acidified inorganic particles (Jang et al., 2002; Tolocka et al., 2004; Gao et al., 2004), in the 1,3,5-trimethylbenzene system in the absence of any seed particles (Kalberer et al., 2004), and in the glyoxal system with both non-acid and acidic seeds aerosols (Liggio et al., 2005a, b).

A number of models have been proposed and developed to predict the SOA formation from aromatic hydrocarbons by using gas–particle partitioning theory. However, these models (1) do not describe or represent particle-phase reactions (Odum et al., 1997; Pun et al., 2002; Dechapanya et al., 2003a, b; Stroud et al., 2004; Griffin et al., 2005); (2) or do not explicitly represent the potential products that lead to SOA formation (Odum et al., 1997; Pun et al., 2002; Dechapanya et al., 2003a, b); (3) or have not been evaluated against smog-chamber data (Pun et al., 2002; Dechapanya et al., 2003a, b); (4) or have questionable ability to simultaneously predict observed SOA, O_3 and NO_x behavior (Johnson et al., 2004, 2005). In this work, a predictive kinetic chemical mechanism for the photo-oxidation of toluene is presented and applied to predict the SOA and ozone formation observed in University of North Carolina (UNC)

dual outdoor aerosol smog chambers. This model is based on atmospheric processes that bring about SOA formation. Particle-phase reactions of some major carbonyl products and gas–particle partitioning processes have been integrated with fundamental gas-phase chemistry. In a companion paper by Hu and Kamens (2007), the model is also evaluated with experimental data sets obtained in different chamber facilities.

2. Experimental section

Experiments were carried out in the UNC $270\,m^3$ dual outdoor aerosol smog chamber facility located in Pittsboro, NC. Chamber descriptions are described elsewhere (Lee et al., 2004). Each chamber half is designated as either north or south. Prior to each experiment, the chambers were continuously flushed with clean rural air for 12–16 h and then purged overnight with dry clean air from a clean air generator. Before the injection of hydrocarbons and oxides of nitrogen (NO_x), an inert gas, sulfur hexafluoride (SF6) was added to the chamber and its concentration was chromatographically measured (Leungsakul et al., 2005b). The loss rate of SF6 over the course of each experiment was used as the dilution rate and applied to all species in the model. Toluene was introduced into the chamber by vaporizing a measured amount of pure liquid toluene (98%, Aldrich, Milwaukee, WI) in a U-tube that was gently heated by a hot air heat gun, and flushed by a dry nitrogen stream. After obtaining the desired toluene concentration, nitric oxide (NO), nitrogen dioxide (NO_2) and, in one case, propylene, were injected into the chamber from high-pressure cylinders. The internal chamber mixing fans were operated during each injection and then shut off 2 min after the injection. This provided uniform chamber concentrations before the start of an experiment. Gas-phase toluene was measured by gas chromatography (GC, Shimadzu Model 14A, column: 30 m, 0.25 mm i.d., J&W DB-1, 0.25 m film thickness) with a flame ionization detector (FID). A liquid nitrogen cryo-trap was used to pre-concentrate gas-phase toluene. Propylene was measured by gas chromatography using a packed column ($2\,m \times 3.2\,mm$ stainless steel with 60–80 mesh, porapak Q at $86\,^{\circ}C$) and an FID for detection. Injected hydrocarbons were sampled every 10 min. Calibrations were performed before each experiment by comparing these with a US National Institute of Standards and Technology traceable

hydrocarbon standard tank. The temperature and humidity of the chamber were continuously monitored during the experiments and these values were used in the model simulations. Detailed descriptions of instruments used for the measurements of NO_x, ozone (O_3), particle, solar irradiance, temperature and humidity are provided elsewhere (Leungsakul et al., 2005a, b).

Gas and particle samples were collected simultaneously by a filter–filter denuder sampling train that consisted of two 47 mm Teflon impregnated glass fiber filters (type T60A20, Pallflex Product Corporation, Putnam, CT) in series followed downstream by a 5 channel 40 cm XAD-4 denuder (University Research Glassware, Chapel Hill, NC). Detailed sample collection and workup procedures are available elsewhere (Leungsakul et al., 2005b).

Gas-phase volatile carbonyls were measured by a standard 1,4-dinitrophenylhydrazene high-pressure liquid chromatography method in some experiments (Grosjean and Fung, 1982). Gas-phase samples were collected onto DNPH cartridges (Supelco, LpDNPH S10) with an ozone scrubber (Supelco) placed upstream. Each sample was taken for 25 min at a flow rate of $0.651 min^{-1}$. The sample workup and analysis procedures are similar to those used by Ho and Yu (2004).

3. Mechanism development

The toluene mechanism was constructed to explicitly represent the formation of first-generation gas-phase products from the photo-oxidation of toluene and further reactions of these products with atmospheric oxidants. We followed the general approach outlined by Calvert et al. (2002) in their review of aromatic atmospheric chemistry. First-generation products are defined as those resulting from initial oxidation of toluene by the hydroxyl (OH) or nitrate (NO_3) radical, and include 1,4-butenedial, 4-oxo-2-pentenal, 2-methylbutenedial, 2-methyl-2,4-hexadienedial, methyl glyoxal, glyoxal, cresol and benzaldehyde. A simple illustration for the formation of first-generation toluene gas-phase products is shown in Scheme 1. Structures for these major gas-phase products are given in Calvet et al. (2002). Semi-explicit mechanisms for these first-generation products were developed and evaluated against outdoor chamber data for 1,4-butenedial, 4-oxo-2-pentenal and cresol (Liu et al., 1999; Johnson et al., 2004). Many of the second-generation products from the photo-degradation of these initial

products have relatively low vapor pressures (10^{-2}–10^{-7} Torr), and thus can partition between the gas and aerosol phases. A kinetic partitioning approach suggested by Kamens et al. (1999, 2001) was used to describe the time-dependent phase distribution of about 70 compounds during the reaction. It is significant that selected heterogeneous reactions of semi-volatile carbonyl compounds (that lead to the formation of large molecules) have also been represented either via calculations of uptake coefficients or by reductions in desorption rate coefficients. This will be discussed in more details later. Rate constants were developed by reference to the available literature (Calvert et al., 2002; Liggio et al., 2005b) and experiment data. Where mechanistic or rate constant information was not available, a structure–activity relationship technique was applied to calculate the gas-phase kinetic parameters (Kwok and Atkinson, 1995), or the mechanistic pathways and rate coefficients from similar compound structures were used (Jenkin et al., 1997; Saunders et al., 2003). The detailed mechanism is available as Supplemental Material. In addition to the toluene mechanism, a Carbon Bond 4 (2002) mechanism was also included that incorporates the reactions of inorganic species (Voicu, 2003). A chamber-dependent auxiliary wall mechanism that describes the background radical sources and sinks of NO_x was also used (Jeffries et al., 1999; Voicu, 2003).

3.1. Gas-phase chemistry

To develop a kinetic mechanism, it is first necessary to characterize the gas-phase reactions that generate semi-volatile oxygenated products. Since abbreviations for many of the product compounds and radicals are used, they are listed in a glossary with their definitions. The main reaction pathway of toluene in the atmosphere is its reaction with the OH radical. The hydroxyl radical can add to the aliphatic toluene carbon and ultimately result in an aldehydic H elimination to form benzaldehyde, or it can add to the benzene ring to form cresol, 2-methyl-2,4-hexendien-dial or a bicyclic peroxy radical, which is called a TOLO2 radical (Calvert et al., 2002). This bicyclic peroxy radical can then undergo a sequence of ring opening and rearrangement reactions to form glyoxal, methyl glyoxal and several unsaturated dicarbonyls (Scheme 1). Recent work has shown that the formation of an epoxide intermediate from
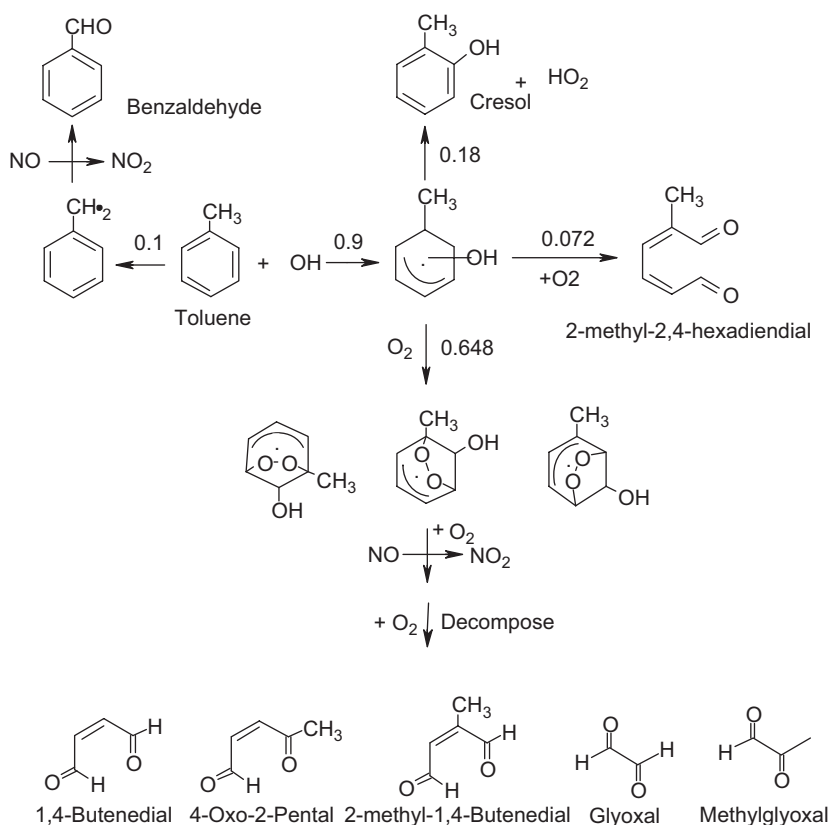
Scheme 1. Simple schematic of OH attack on toluene and the formation of first-generation products. Cresol represents a mixture of *o*-, *m*- and *p*-Cresol isomers.

OH-initiated reaction of toluene was not kinetically favorable and was negligible by comparison to the formation of TOLO2 (Suh et al., 2003). Thus the epoxy-oxy route of toluene degradation is not included in this mechanism (Barnes et al., 1996; Yu et al., 1997; Bloss et al., 2005).

The general approach to generating our mechanism and the Master Chemical Mechanism (MCM) by Johnson et al. (2004) is similar in that both explicitly represent the initial formation of toluene ring and ring cleavage products. We start, however, with branching ratios of OH addition to the *ortho*, *meta*, *para* and *ipso* positions of toluene that were recommended by Suh et al. (2003) as 0.52, 0.11, 0.34 and 0.03, respectively. If the addition to *ipso* position is ignored, the products yields from the ring opening reaction of TOLO2 are 0.265 for 1,4-butenedial, 0.313 for 4-oxo-2-pentenal, 0.422 for 2-methyl-1,4-butenedial, 0.735 for glyoxal and 0.265 for methyl glyoxal. Different laboratory studies of toluene products suggest, however, that the amounts of glyoxal and methyl glyoxal formed

from toluene are about the same (Calvert et al., 2002). Therefore, based on available experimental measurements and our best model fits, the yields of 1,4-butenedial, 4-oxo-2-pentenal, 2-methyl-1,4-butenedial, glyoxal and methyl glyoxal were set to be 0.60, 0.25, 0.15, 0.40 and 0.60, respectively.

As with other aromatic models (Johnson et al., 2004, 2005), the simulation of toluene decay later in the reaction was a challenge. It was found that the simulated OH concentration was insufficient to account for the removal of toluene and cresol as O_3 was accumulating. One possible pathway is the recently proposed reaction by Broyles and Carpenter (2005) between alkyl peroxy radicals (RO_2) and benzene to give a benzene epoxide as is illustrated in (Rxn.1).
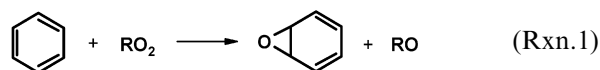
Compared to saturated RO_2 radicals, unsaturated RO_2 radicals have lower O–O bond dissociation

energies and these may favor the formation of the aromatic epoxide. Model simulation of the toluene decay was dramatically improved after this reaction pathway was incorporated into the mechanism and was represented by the reactions of toluene with unsaturated acyl peroxy radicals. Since toluene oxide is formed by this reaction, it also explains the observation of benzene oxide analogues observed in the product studies of aromatic hydrocarbons (Kwok et al., 1997; Yu et al., 1997).

Ozonolysis of unsaturated dicarbonyls takes place at the unsaturated double bond to give glyoxal, methyl glyoxal and an excited Criegee intermediate (Liu et al., 1999). Ozonolysis rate constants of 1.6×10^{-18} and $4.8 \times 10^{-18}\,cm^3$ molecule^{-1}s^{-1} as measured by Liu et al. (1999) are used for 1,4-butenedial and 4-oxo-2-pentenal, respectively. Hydroxyl radicals react with unsaturated dicarbonyls by either effectively abstracting the aldehydic hydrogen, or adding to the unsaturated double bond to produce a host of alkyl radicals (R). The R radicals are oxidized quickly by atmospheric O_2 to form RO_2 radicals. These RO_2 radicals can then react with NO, NO_2, hydroperoxy radicals (HO_2) and other RO_2 radicals to form the second-generation products. Upon reacting with NO, an alkyl nitrate ($RONO_2$) or an alkoxy radical (RO) and NO_2 are formed. Where data were not available, the yield of organic nitrate was estimated to be the same as that for the corresponding unsubstituted alkyl RO_2 except for acylperoxy RO_2 radicals. The alkyl nitrate formation yield for acylperoxy RO_2 was taken to be zero as per Jenkin et al. (1997). These yields were used as a guide to adjust the mechanism parameters to give a best fit to the NO_x–O_3 and SOA concentration time profiles.

All the second-generation products may react with OH to form third-generation products. Unfortunately, the literature that is related to the photochemistry of the highly oxygenated products of toluene is very limited. It is assumed that the photolysis rate coefficients of the highly oxygenated second- and third-generation products are very small and thus to be unimportant. This includes compounds such as C4 ketoaldehydes (C4KETALD) and C5 ketoaldehydes (C5KETALD). MCM tends to explicitly describe the chemistry of second- and third-generation products. For computational efficiency, we grouped and lumped these compounds according to their carbon number and function groups. For example, C5OHACID represents all acids with five carbons, one hydroxyl and two ketone groups. If we were to explicitly represent a carboxylic acid with five carbons, one hydroxyl and two ketone groups, and have the OH group on the second, third or fourth carbon, current techniques would not predict any change in reactivity.

A scalar parameter called TRO_2, which is the sum of all alkylperoxy radicals, is defined in the mechanism and is computed before any radical–radical reactions. Instead of having explicit RO_2 cross-reactions, each individual RO_2 was reacted with TRO_2 to yield products specific to RO_2. This saved over 400 reaction steps in the mechanism compared to explicitly representing each $RO_2 + R_iO_2$ reaction, where R_iO_2 represents all of the other individual RO_2 radicals.

3.2. Particle-phase chemistry

3.2.1. Nucleation

A chamber experiment with natural morning sunlight and 1.0 ppmV of toluene in the presence of 4 ppb of NO_x showed a rapid generation of self-nucleated particles in the 5–12 nm range (Fig. 1). This occurred in the presence of background particles with diameters of 35–200 nm that existed in the chamber as background aerosols and had a total mass loading of about 8 μg m^{-3}. The composition of these background aerosols, although not determined in this experiment, was assumed to be largely inorganic sulfates and nitrates (Leungsakul et al., 2005b). Before NO_x injection, toluene may have reacted with background hydroxyl radical to form cresol, benzaldehyde, 2-methyl-2,4-hexadienedial and TOLO2. In chamber experiments with natural sunlight, a particle burst was observed from the photolysis of hexendiendial after exposure to sunlight for 10–25 min (Klotz et al., 1999). A 2-butenal-4-yl-ketene was proposed as the photolysis product. Similar to hexendiendial, the 2-methyl-2,4-hexadienedial, MHEXDIAL, is assumed to photolyse and form 2-methyl-2-butenal-4-yl-ketene, which is called C7KETENE in the mechanism. This C7KETENE has an alkene carbon double bond, so it can easily undergo a classical organic 2+2 ketene-alkene cycloaddition reaction with another C7KETENE to form a cyclobutanone derivative (Grossman, 1999). This product has one ketene group, one carbon double bond and three carbonyl groups, and is called C14KETENE in the mechanism. C14KETENE is then allowed to dimerize to give a particle nuclei, SEED1, with an estimated vapor pressure of 10^{-21} Torr (Mackay et al., 1982; Stein and Brown, 1994; Zhao et al., 1999) and is considered non-volatile.
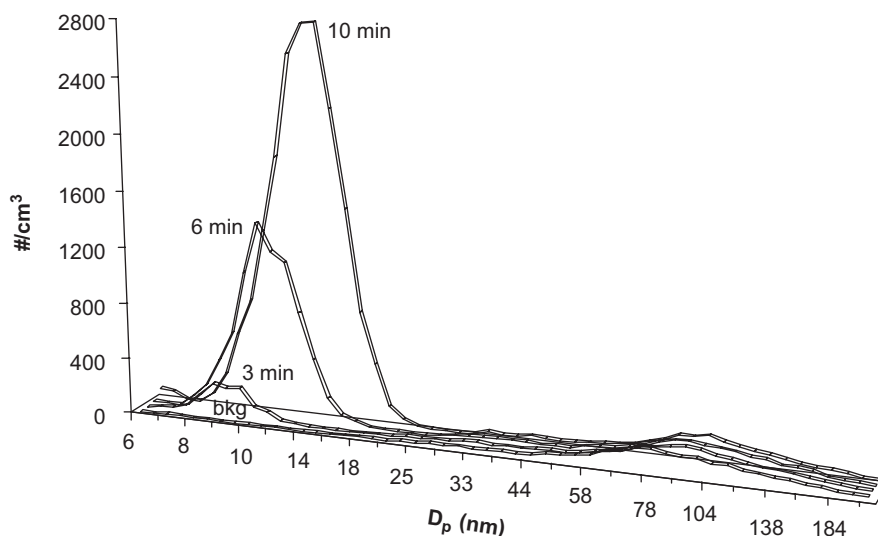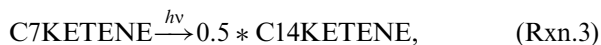
Fig. 1. Nucleation of toluene reaction products in the presence of background aerosols that are observed from 11504N. D_p is particle diameter.

This reaction is speculative and needs to be verified analytically. Its formation rate was derived empirically from the initial increase of particle numbers that was observed in a toluene-sunlight chamber experiment in the absence of NO:

$$\text{MHEXDIAL} \xrightarrow{h\nu} \text{C7KETENE}, \qquad (\text{Rxn.2})$$

$$\text{C7KETENE} \xrightarrow{h\nu} 0.5 * \text{C14KETENE}, \qquad (\text{Rxn.3})$$

$$\text{C14KETENE} + \text{C14KETENE} \rightarrow \text{SEED1}. \qquad (\text{Rxn.4})$$

3.2.2. Gas–particle partitioning

A kinetic approach was used to represent the gas–particle partitioning processes (Kamens et al., 1999; Kamens and Jaoui, 2001). This approach incorporates gas–particle partitioning with gas-phase kinetics by explicitly expressing absorption and desorption of each semi-volatile partitioning species. An example of the C5OHACID partitioning sequence is illustrated in (Rxns. 5 and 6):

$$\text{C5OHACID} \rightarrow \text{C5OHACIDP} + \text{SEED} \quad k_{\text{on}}, \qquad (\text{Rxn.5})$$

$$\text{C5OHACIDP} \rightarrow \text{C5OHACID} \quad k_{\text{off}} \qquad (\text{Rxn.6})$$

where k_{on} is the rate of absorption, k_{off} is the rate of desorption and C5OHACID and C5OHACIDP are the gas and particle phases of a C5

hydroxycarboxylic acid. To reduce the number of gas–particle partitioning cross-reaction steps, a scalar parameter TSP (similar to TRO$_2$) was introduced into the mechanism, which is the sum of all particle-phase products and is computed at each time step. Instead of letting the gas-phase semi-volatile compound explicitly partition onto each particle-phase species, one pseudo first-order reaction was used to represent all these reactions with a rate coefficient of $k_{\text{on}} \times \text{TSP}$. If there are 20 partitioning species, this reduces the number of partitioning reaction steps by 20^2–20, or 380 steps.

$$\text{C5OHACIDG} \rightarrow \text{C5OHACIDP} \quad k_{\text{on}} \times \text{TSP}. \qquad (\text{Rxn.7})$$

Semi-volatile products generated in the gas phase are assumed to be governed by equilibrium between the liquid particle phase and surrounding gas phase. At equilibrium, the gas–particle partitioning equilibrium constant ^iK_p (m^3 µg^{-1} of particle mass) equals to the ratio of k_{on} over k_{off}. The equilibrium constant (m^3 µg^{-1}) may be theoretically estimated from the absorption model of Pankow (1994)

$$^iK_p = (760RTf_{\text{om}})/(^ip_L^{Oi}\gamma_{\text{om}}10^6\,\text{MW}_{\text{om}}), \qquad (1)$$

where T is the temperature (K), f_{om} is the mass fraction of organic material (om) in particulate matter, MW_{om} is the average molecular weight of a given liquid medium (g mol^{-1}), $^i\gamma_{\text{om}}$ is the activity coefficient of a given organic compound, i, in a given organic mixture, $^ip_L^O$ is the saturated liquid

vapor pressure in Torr and R is the gas constant in $m^3 \, atm \, mol^{-1} \, K^{-1}$. A value of unity for ${}^i\gamma_{om}$ was assigned to all partitioning species as the aerosol phase is assumed to be composed of similar types of compounds (Kamens et al., 1999; Leungsakul et al., 2005a).

The desorption rate of a compound from a bulk liquid surface has been previously estimated (Kamens et al., 1999; Kamens and Jaoui, 2001; Yasuoka et al., 1994; Matsumoto et al., 1994):

$$k_{off} = \frac{k_b T}{h} \exp\left(-\frac{E_a}{RT}\right), \qquad (2)$$

where k_b is Boltzmann's constant ($1.381 \times 10^{-23} \, J \, K^{-1}$), h is Planck's constant ($6.626 \times 10^{-34} \, J \, s$), T is temperature (K), R is the universal gas constant in $8.314 \, J \, K^{-1} \, mol^{-1}$ and E_a (Glasstone et al., 1941) is the activation energy or energy barrier required for desorption from the particle ($J \, mol^{-1}$). For compounds that could participate in particle-phase reactions and with sub-cooled liquid vapor pressure, ${}^i p_{L,298\,K}^O$, higher than $10^{-3} \, Torr$, their E_a values were estimated from vapor pressures, which will be discussed in more detail in the next section. For all the other products, their E_a values were estimated from the vapor pressure relationship of Kamens et al. (1999) and Kamens and Jaoui (2001).

The absorption rate constant k_{on} can be then calculated by

$$k_{on} = {}^i K_p \times k_{off}. \qquad (3)$$

Because it is difficult to obtain actual vapor pressures for most semi-volatile products, we have used an approach proposed by Mackay et al. (1982) to estimate liquid vapor pressure from the boiling points (T_b) and entropies of vaporization (ΔS_{vap})

$$\ln p_L^O = \frac{\Delta S_{vap}}{R}\left[(1.8)\left(1 - \frac{T_b}{T}\right) + (0.8)\left(\ln\frac{T_b}{T}\right)\right], \qquad (4)$$

where ΔS_{vap} is in $J \, mol^{-1} \, K^{-1}$, T_b is in K and R is the universal gas constant ($8.31 \, J \, mol^{-1} \, K^{-1}$).

The normal boiling point can be estimated using the Joback and Reid (1987) extended group contribution method to cover more groups, and corrected for a temperature-dependent bias (Stein and Brown, 1994). The entropy of vaporization has been computed based on a group contribution method (Zhao et al., 1999). Because organic nitrates typically have higher vapor pressures than are estimated by the above techniques, the estimation

method of Nielsen et al. (1998) was used for organic nitrates.

3.2.3. Particle-phase reactions

Recent laboratory studies have found that pre-existing acidic particles can promote particle-phase reactions of aldehydes and ketones and lead to higher SOA yields than non-acidic particles (Jang et al., 2002, 2003). Oligomer structures have been characterized not only in α-pinene/ozone systems with acidic seeds (Tolocka et al., 2004), but also as proposed in a 1,3,5-trimethylbenzene/propylene/NO_x system in the absence of any seed aerosol (Kalberer et al., 2004). We have implemented after Kalberer et al. (2004) and Offenberg et al. (2006) a "hot-DMA" technique in which SOA generated in our chambers are heated in a manifold before they are sized with a long differential particle mobility analyzer (DMA) and associated condensation nuclei counter (CPC SMPS-TSI). We have found that after raising the aerosol bath gas temperature from ambient to $100\,^\circ C$ for a period of 0.13 s, ~90% of the toluene aerosol volume/mass remains. This is consistent with the recent detailed outdoor chamber toluene SOA products analysis work by Hamilton et al. (2005), where these investigators only account for at most 10% of the toluene SOA in C3–C7 oxygenated products. Using Eq. (2), and the E_a vapor pressure relationship (Kamens et al., 1999), one can estimate that the compounds "off gassing" from the newly formed toluene SOA at $100\,^\circ C$ have a composite vapor pressure at $25\,^\circ C$ in the range of $10^{-8} \, Torr$. In addition, from other experiments, we have shown that the aerosol volume remaining at $100\,^\circ C$ for the toluene system is much greater than that observed for the 1,3,5-trimethylebenzene (1,3,5-TMB) system (Kalberer et al., 2004). This suggests a higher degree of polymerization for the toluene–SOA system than for the 1,3,5-TMB system. Like Kalberer et al. (2004), we observed an increase in the amount of aerosol volume remaining over time after passing through the heated DMA manifold. This also suggests that with time the aerosol is composed of less volatile and probably more highly oligomerized compounds.

The reactive uptake of simple aldehydes onto particular matter has recently been investigated (Liggio et al., 2005b; Kroll et al., 2005). Glyoxal, which is one of the major gas-phase products formed from toluene gas-phase oxidation, was observed to have a large uptake onto both acidic and non-acidic aerosol. An uptake coefficient of

glyoxal that ranges from 8.0×10^{-4} to 7.3×10^{-3} was given for $(NH_4)_2SO_4$ seed aerosols at 55% relative humidity (Liggio et al., 2005b). Although the uptake coefficient was related to particle acidity and humidity, it was suggested that the glyoxal uptake may not be a result of particle acidity but rather of the ionic strength of the seed (Kroll et al., 2005). In our current mechanism, the reactive uptake of glyoxal is represented by

$$GLY \rightarrow 0.4 \times GLYPOLY, \quad k_{part\_gly}, \qquad (Rxn.8)$$

where GLY is gas-phase glyoxal, GLYPOLY is particle-phase glyoxal oligomer with a molecular weight that is equal to the average of $(C_2H_2O_2)_2(H_2O)_2$ and $(C_2H_2O_2)_3(H_2O)_2$ (Liggio et al., 2005b), and the factor of 0.4 is used to keep the carbon number balance. As per Liggio et al. (2005b), the overall loss rate of gas-phase glyoxal can be expressed as

$$\frac{dC_g}{dt} = -\gamma \pi a^2 \langle c \rangle C_g N_p = k_{part\_gly} C_g, \qquad (5)$$

where γ is the uptake coefficient, a is the particle radius, $\langle c \rangle$ is the mean molecular speed of the gas, C_g is the gas-phase concentration of glyoxal and N_p is the particle number concentration. For mono-disperse particles, the particle surface concentration S, equals $4\pi a^2 N_p$. Since we can easily relate S to particle mass concentration, the overall uptake rate of gas-phase glyoxal can then be calculated as a function of total particle mass concentration:

$$k_{part\_gly} = \frac{6.0 \times 10^{-12} \gamma \langle c \rangle TOM}{4 d_p D_p}, \qquad (6)$$

where TOM is the organic particle mass concentration ($\mu g\,m^{-3}$), d_p is particle density ($g\,cm^{-3}$), D_p is the mean particle diameter (cm) and $\langle c \rangle$ is the mean molecular speed of glyoxal gas (we estimate $3.25 \times 10^4\,cm\,s^{-1}$). An uptake coefficient of 5.7×10^{-4} was used in model simulations based on its reasonable fit to all experimental conditions, although this value is smaller than the uptake coefficients recommended by Liggio et al. (2005b) for a pure glyoxal system with inorganic seed aerosol. The SOA formed in the toluene/NO_x system has a much more complicated speciation than that formed in the glyoxal system. The reaction of glyoxal with other toluene oxygenated products in the particle phase may not be as favorable as its reaction with the hydrated glyoxal analogues. Therefore, it is reasonable to assume that with the same amount of organic mass, less glyoxal uptake

onto the toluene SOA will occur than with pure glyoxal aerosol. Although methylglyoxal was observed to have no uptake onto seed aerosol by Kroll et al. (2005), it was identified as the most significant participant in particle-phase oligomers formation in a 1,3,5-trimethylbenzene/propylene/NO_x system (Kalberer et al., 2004). So the reactive uptake of methylglyoxal is represented in a similar way to glyoxal in the mechanism. Since there is only one aldehydic carbon in methylglyoxal, we assumed it would be more difficult for it to undergo dimmer and trimerization then glyoxal. In addition, when we varied the scaling factor from 0.1 to 0.5, it did not significantly impact SOA prediction. Therefore, a middle value of 0.3 was assumed.

Particle-phase reactions between organic peroxides (ROOH) and aldehydes (R'CHO) that lead to the formation of peroxyhemiacetals (ROOC(OH)R'H) are represented in the updated MCM version 3.1 (Johnson et al., 2004, 2005). These peroxyhemiacetals have estimated vapor pressures lower than 10^{-12} Torr, and, once formed, they tend to stay in the particle phase. At $86\,°C$, the reaction of ROOH and R'CHO leads to a carboxylic acid and an alcohol rather than the peroxyhemiacetal product. This is the well-known peroxide-induced Baeyer–Villiger oxidation (Lehtinen et al., 2001). At room temperature, the peroxyhemiacetal intermediate forms in the concentrated liquid phase (Durham et al., 1958). The extent of this reaction in the gas phase in unknown; hence we have assumed the formation of peroxyhemiacetals to be surface or liquid phase mediated. Given reasonable estimates of the partitioning of most of the organic peroxides and aldehydes from the toluene system, huge aerosol phase reaction rate coefficients for the reaction between ROOH and R'CHO to form peroxyhemiacetals would be needed. For this to be the case, we would also have to argue that uptake coefficients of organic peroxides are extremely high. This is unknown and highly speculative. In the current mechanism, neither the formation of gas-phase peroxyhemiacetals nor the formation of the carboxylic acid from the reaction of organic peroxides in the liquid phase is included. This is because at this stage, very little is known about the kinetics of these reactions.

There may be other possible particle-phase reaction pathways in addition to the previously proposed reaction mechanisms of hydration, hemiacetal and acetal formation, aldo-condensation and polymerization (Jang and Kamens, 2001a; Kalberer

et al., 2004; Tolocka et al., 2004; Gao et al., 2004). Unfortunately at this time, we are not able to explicitly represent these particle-phase reactions in the toluene mechanism due to the lack of information about their kinetic data and products. Instead, an "apparent" E_a value has been applied to each oxygenated product that could participate in the particle-phase reactions to derive an overall off-gassing rate constant k_{off}, which accounts for both thermodynamic partitioning and particle-phase chemical reactions. Using de nuders, particle desorption rates for five toluene aerosol phase products have been investigated and a linear relationship between their activation energies, E_a, and the log values of their sub-cooled vapor pressures at 298 K, log $^i p^O_{L,298 K}$, was derived:

$$E_a(\text{kJ mol}^{-1}) = -0.7088 \times \log{(^i p^O_{L,298 K}/\text{Torr})}$$
$$+ 73.645, \quad r^2 = 0.887. \quad (7)$$

It was observed that products with liquid vapor pressures, $^i p^O_{L,298 K}$, higher than 10^{-3} Torr, had larger E_a values and smaller k_{off} than those obtained using our previous relationship derived for non-polar compounds (Kamens et al., 1999). This suggests that these products take part not only in gas–particle partitioning but also in particle-phase reactions. Therefore, k_{off} for 18 partitioning carbonyl, acid and organic peroxide products with $^i p^O_{L,298 K}$ higher than 10^{-3} Torr were calculated from the new relationship between E_a and log $^i p^O_{L,298 K}$. The net result, however, was not very significant because the actual partitioning of these compounds to the particle phase, even with this new relationship, did not dramatically increase.

3.3. Chamber wall chemistry

For experiments performed in smog chambers, it is known that the heterogeneous processes occurring on the walls of the chamber can have significant impact on the chemical system under observation (Killus and Whitten, 1990; Carter et al., 1981). To use smog-chamber data to develop and evaluate our chemical mechanism, a UNC auxiliary mechanism is included to represent the chamber-related effects (Jeffries et al., 1999; Voicu, 2003). A series of characterized experiments were performed to quantify the physical properties and chemical reactivity of the UNC 270 m³ dual outdoor aerosol smog-chamber walls, which include NO_x/O_3 decay, matched propylene with NO_x, matched ethylene

with NO_x, matched formaldehyde and matched particle decay experiments. Wall loss rates for all gas-phase compounds are estimated from vapor pressures as per Kamens et al. (1999). The average dark O_3 loss rate corrected for dilution is $7.53 \times 10^{-7} \text{s}^{-1}$ for each half of the 270 m³ dual chambers. A first-order wall loss rate of $1.023 \times 10^{-5} \text{s}^{-1}$ is observed for particle decay in the dark, and is used to correct for particle deposition to the wall for all experiments. The residence time of gas-phase compounds in the sampling line is 1 s, and is used to correct a difference between observed and measured O_3 and NO_x concentrations due to reactions in the sampling line.

4. Results and discussion

4.1. Particle mass

A comparison between calculated SMPS data and measured gravimetric particle mass concentrations for an experiment on 16 October 2004 in the north chamber (101604N) is illustrated in Fig. 2. It is shown that, with a particle density of 1 g cm⁻³, the calculated SMPS mass is lower than gravimetric filter mass. A density of 1.4 g cm⁻³ was recommended by Bahreini et al. (2005) for many SOA systems. If this factor is applied to correct the SMPS data, a very good agreement between the SMPS mass and measured filter mass is observed. For SOA model comparisons, when available, we have presented aerosol mass concentrations derived from both the front filter data and the front filter masses adjusted by subtraction of the masses collected on the second or backup filters. We believe the true mass lies somewhere between these two representations of the particle mass concentrations. For the dual experiments on 27 July 2005 (072705N and 072705S in Table 1), the experimental particle concentration was so low that measured filter masses did not provide useful trends. Since the particle size distributions on this day were within the DMA range, the SMPS mass concentrations corrected by a factor of 1.4 were used for model comparisons.

4.2. Reaction of NO₂ with particle-phase water

In the initial development of the toluene–SOA mechanism, typically simulation results showed an over-prediction of the measured ozone after it

reached its maximum concentration in the afternoon (Fig. 3). As ozone is generated by the photolysis of NO_2, ozone production is mainly affected by the conversion of NO to NO_2 and the loss of NO_x into stable nitrogen compounds. To correct for the excess ozone formation, one could try to reduce the production of RO_2 and HO_2 to let more NO be oxidized to NO_2 by ozone, but this
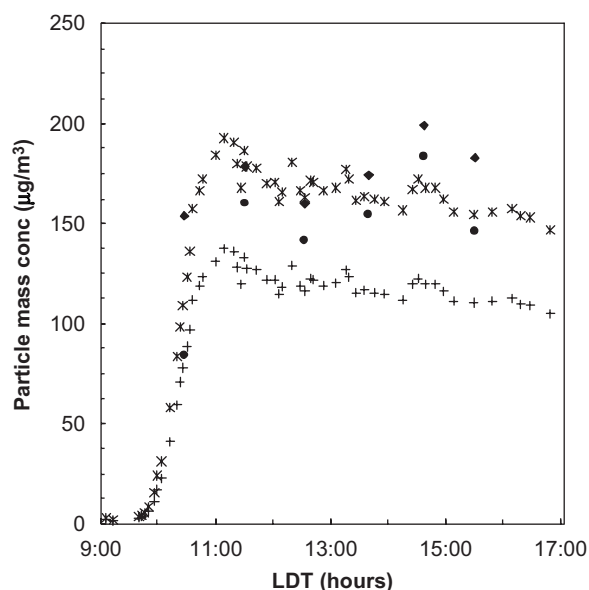
would also reduce OH formation and thus decrease the oxidation capacity of the system. Therefore, the over-prediction of ozone by the model may be due to additional, but unknown reactions that sink NO_x into stable NO_y species, other than the formation of organic nitrates ($RONO_2$), organic acylperoxy nitrates ($RCO–OONO_2$), peroxyacetyl nitrate (PAN) and nitric acid (HNO_3).

Organic acylperoxy nitrates serve as temporary NO_2 reservoirs in the system. As temperature increases, they undergo thermal decomposition to give back NO_2. The thermal decomposition rate constant of α-pinonyl peroxy nitrate formed from the α-pinene system (Noziere and Barnes, 1998) and the formation rate of PAN are used as the decomposition and formation rates for all organic acylperoxy nitrates in the developed toluene mechanism. These rates are directly related to NO_2 concentrations in the afternoon and influence ozone production. However, increasing the formation rate constant by a factor of two did not decrease simulated ozone concentrations significantly.

Another option to remove gas-phase NO_x would be to shunt more into organic nitrates from the reaction of RO_2 radicals with NO. Model simulation of the gas-phase degradation of 1,4-butenedial showed that increasing the yield of organic nitrates from 0.14 to 0.4 did not improve the overestimated simulations of experimental O_3 concentrations, whereas it greatly over-predicted the SOA mass concentrations. Speciation of simulated aerosol material shows that the two most significant organic nitrate species in the particle phase, called RgDOH-NO3 and RgTOHNO3, come from cresol degradation in the mechanism. Increasing their formation yield from 0.14 to 0.4 lowered the simulated ozone

Fig. 2. Comparison between calculated SMPS masses and gravimetric masses for 101604N. LDT is local daylight saving time. Solid squares represent uncorrected front filter mass concentrations; solid dots represent filter mass concentrations corrected by backup filter subtraction; asterisks (∗) represent calculated SMPS particle mass concentrations by assuming aerosol density of $1.4\,g\,cm^{-3}$; plus (+) represents calculated SMPS particle mass concentrations by using a density of $1.0\,g\,cm^{-3}$.

Table 1
Experimental conditions used to develop and evaluate the toluene mechanism

Experimental date	Initial concentration (ppm)					Dew point (K)
	$[Tol]_0$	$[NO]_0$	$[NO_2]_0$	$[Tol]_0/[NO]_0$	Temp (K)	
052204S[a]	0.992	0.445	0.088	2.23	303–314	294–295
092304N	0.500	0.204	0.014	2.45	296–307	292–294
092304S	0.980	0.280	0.026	3.50	296–307	291–295
101604N	1.023	0.096	0.014	10.66	288–300	277–282
101604S	0.540	0.370	0.027	1.46	288–300	277–282
111504N	0.864	0.272	0.055	3.18	284–294	274–276
072705N	0.186	0.091	0.039	2.04	300–310	276–281
072705S	0.095	0.091	0.042	1.04	300–310	278–283

[a]One ppm V of propylene was also injected into the chamber.
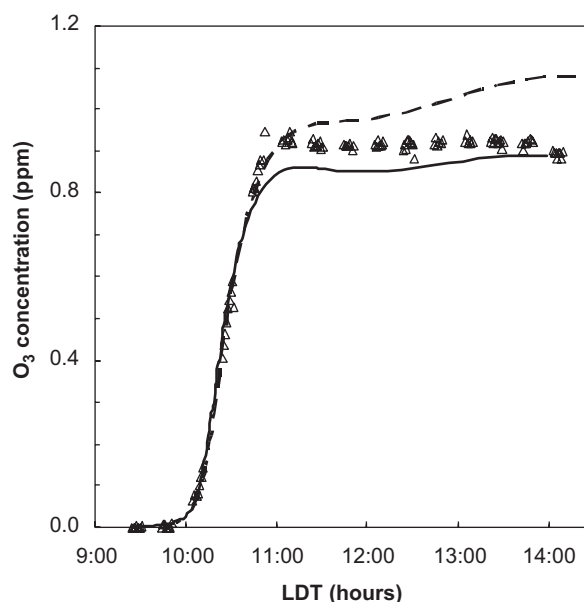
Fig. 3. Comparison of simulated and measured O_3 concentration for 052204S by using two versions of toluene mechanisms. The dashed line (−−) is simulated O_3 concentration by using a toluene mechanism without the reactions of NO_2 with aerosol phase reaction; the solid line (—) is the simulated O_3 concentration by using a toluene mechanism with the reactions of NO_2 with particle-phase water; triangles ($\triangle$) represent measured O_3 concentrations.

concentration by less than 10% for all experiments, but greatly increased the predicted aerosol mass. This was especially true for the low-concentration systems, the model over-predicted particle mass by 57% for 072705S after this change. This indicated that there must be other reaction channels that can remove excess NO_2 in the toluene system, but are yet unknown.

In our current mechanism to represent the needed additional loss of NO_2, NO_2 is converted to aerosol phase HNO_3 by reacting it with particle-phase water. This process is represented in a similar way to the conversion of NO_2 to wall HNO_3 by wall reactions. The formation rate of particle-phase HNO_3 was chosen based on the best model fit. The liquid water content in the particle phase can be estimated as a function of relative humidity inside the chamber as per Jang and Kamens (1998). Although just a minor fraction of afternoon NO_2 is tied up in the particle phase (about 0.7% in high-concentration runs and 0.1% in low-concentration runs), it greatly improved the model simulation of ozone profile for most runs as illustrated in Fig. 3.

4.3. Simulation results

Eight experiments performed in the UNC 270 m^3 dual outdoor aerosol smog chambers are simulated to demonstrate the model performance and to examine the influence of various physical and kinetic parameters. Experimental conditions are shown in Table 1. Initial toluene concentrations range from 0.095 to 1.023 ppm V, NO from 0.091 to 0.445 ppm and the initial concentration ratios of toluene to NO range from 1.04 to 10.66. Temperatures ranged from 284 to 314 K, dew points from 274 to 295 K and solar conditions from May to November. Only toluene and NO_x were injected into the chamber for most of the experiments except for the 052204S experiment, where 1.0 ppm V propylene was also injected.

Background hydrocarbon concentrations inside the chamber were measured at the start of each experiment and the total concentration was less than 50 ppb C with toluene concentrations being less than 5 ppb C or 0.7 ppb V. Initial NO_x (NO + NO_2) in the chamber was less than 10 ppb. In the model, the reactivity of outdoor exchanged background volatile organic carbon (BVOC) with chamber air is represented by Jeffries et al. (1998):

$$OH + BVOC \rightarrow 0.667 * (XO_2 + FORM + HO_2)$$
$$+ 0.167 * C_2O_3 + 0.001 * PAR,$$
$$(Rxn.9)$$
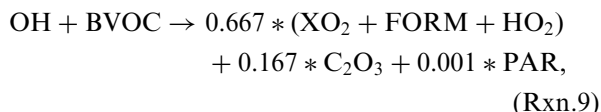
where FORM is formaldehyde, C_2O_3 is an acyl peroxy radical, PAR is a paraffin and XO_2 is a generalized radical that implicitly accounts for the oxidation of NO to NO_2, and RO_2 to RO. A second-order rate coefficient of 3.0×10^{-12} cm^3 molecule^{-1} s^{-1} is used. The impact of background hydrocarbons and NO_x on the simulation, given the relatively high starting concentrations of toluene and NO_x, is negligible.

Comparisons between experimental data and model simulations are shown in Fig. 4. Fits that were within ± 5% of the data are called "very good" fits (or "fits very well"); fits that were within ± 15% are called "good" (or "tracks well"); and fits within ± 30% are called "reasonable" (or "reasonable fits or tracks"). Generally, the model predicts the decay of toluene very well for most conditions except for 052204S, 092304N and 111504N, where the model overestimates the loss of toluene by about 17%. The model also tracks the NO–NO_2 conversion very well and it fits the ozone concentration

profiles for all high toluene concentration runs reasonably well. The model tends to over-predict afternoon ozone concentrations by about 30% for the low-concentration systems (i.e. 072705N and 072705S). It should be noted that the SOA masses formed in these two systems are low compared to those in the high-concentration systems, where the maximum aerosol mass concentrations are $16\,\mu g\,m^{-3}$ for 072705S and $33\,\mu g\,m^{-3}$ for 072705N. Under these low aerosol mass conditions, the

amount of water in the particle phase would be too low to convert all the excess NO_2 in the system into particle-phase HNO_3. This suggests that there may be other reaction pathways that can remove excess NO_2 in the afternoon in the toluene/NO_x system.

With respect to particle formation, our new UNC toluene mechanism reasonably tracks experimental SOA formation except for 101604N, where the model does not do a good job of simulating the
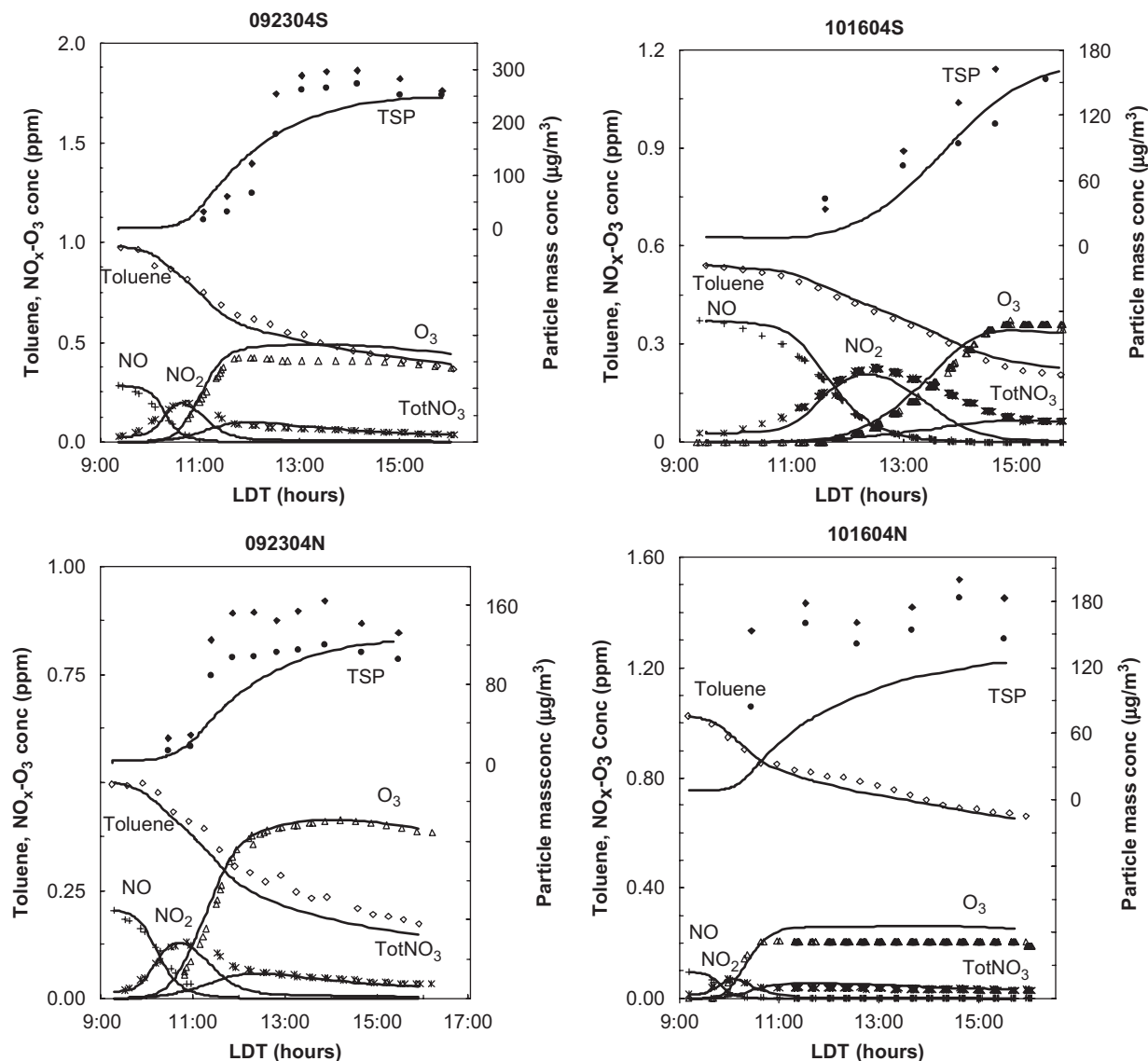
Fig. 4. Comparison of model simulated and measured concentrations of toluene, NO_x, ozone and aerosol for eight toluene/NO_x experiments. The solid lines (—) represent model simulations. The plus (+) are measured NO; asterisks (∗) are measured NO_2; triangles (△) are measured O_3; diamonds (◇) are measured toluene; solid diamonds (◆) are measured front filter mass; solid circles (●) are filter masses corrected by backup filter subtraction; and squares (□) are calculated SMPS particle mass concentrations by assuming a density of $1.4\,g\,cm^{-3}$.
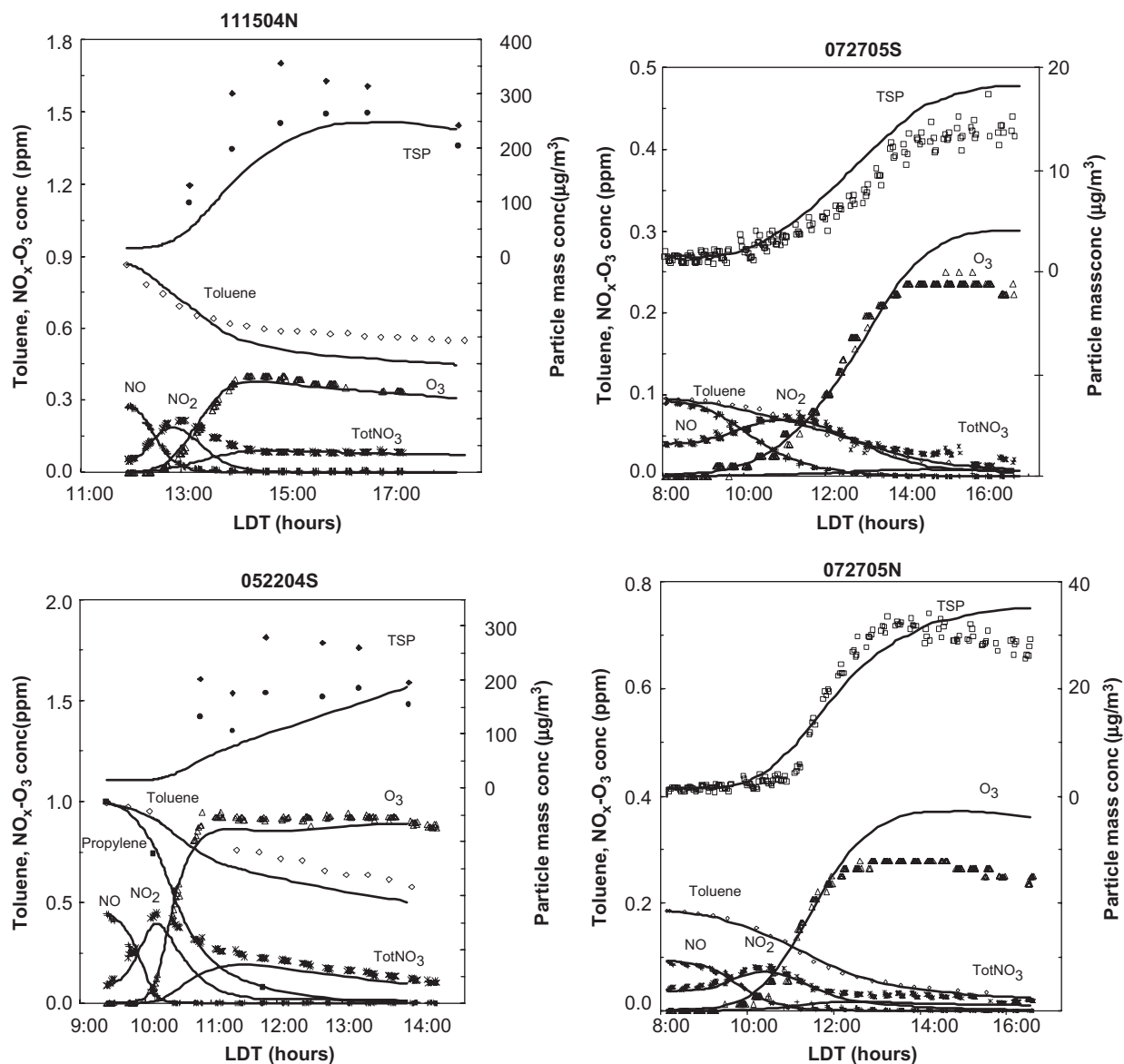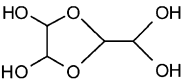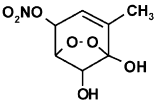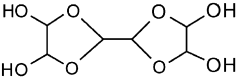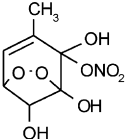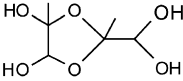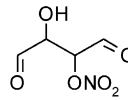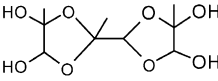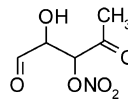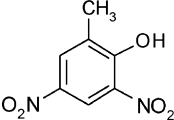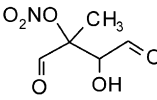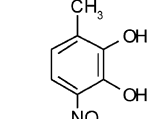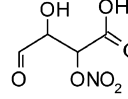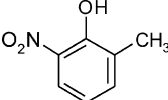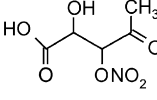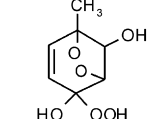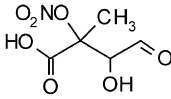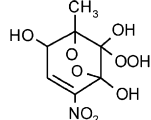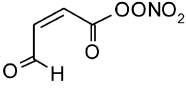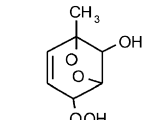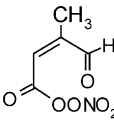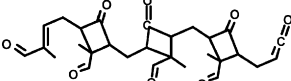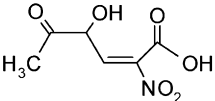
Fig. 4. (*Continued*)

rapid initial particle growth and hence under-estimates the aerosol mass concentrations. The model also tends to under-predict the initial particle burst to different extents for almost all high-concentration experiments, whereas it over-predicts the initial particle generation for the low-concentration runs. In the mechanism, ketene oligomers (SEED1) from the photolysis of 2-methyl-2,4-hexadienedial, together with the background chamber aerosol, SEED, provide the only available initial particle surfaces for semi-volatile species to partition between the gas and aerosol phases. As will be discussed later, the mass

fraction of SEED1 is higher in the low-concentration systems than that in the high-concentration systems. This indicates that there must be some other unknown reaction pathways that can also contribute to the initial particle formation.

The dominant particle-phase species predicted by the mechanism are glyoxal oligomers (GLYPOLY), SEED1, organic nitrates, methyl nitro-phenol analogues, C7 organic peroxides, acylperoxy nitrates and, for the low-concentration experiments, unsaturated hydroxyl nitro acids (C6OHNO2ACID). Their molecular structures are shown in Table 2. As is illustrated in Fig. 5, the relative amounts of these

Table 2
Chemical structures of major model-simulated aerosol phase species

Name[a]	Structure	Name[a]	Structure
GLYPOLY		RgDOHNO3	
MGLYPOLY		RgTOHNO3	
		ROHALDNO3	
RgOHDINO2			
RgDIOHNO2		ROHALDACIDNO3	
RgOHNO2			
CROHOOH			
RgTOHNO2OOH		BUDACIDONO3	
TOLOOH		MBUDACIDONO3	
SEED1		C6OHNO2ACID	

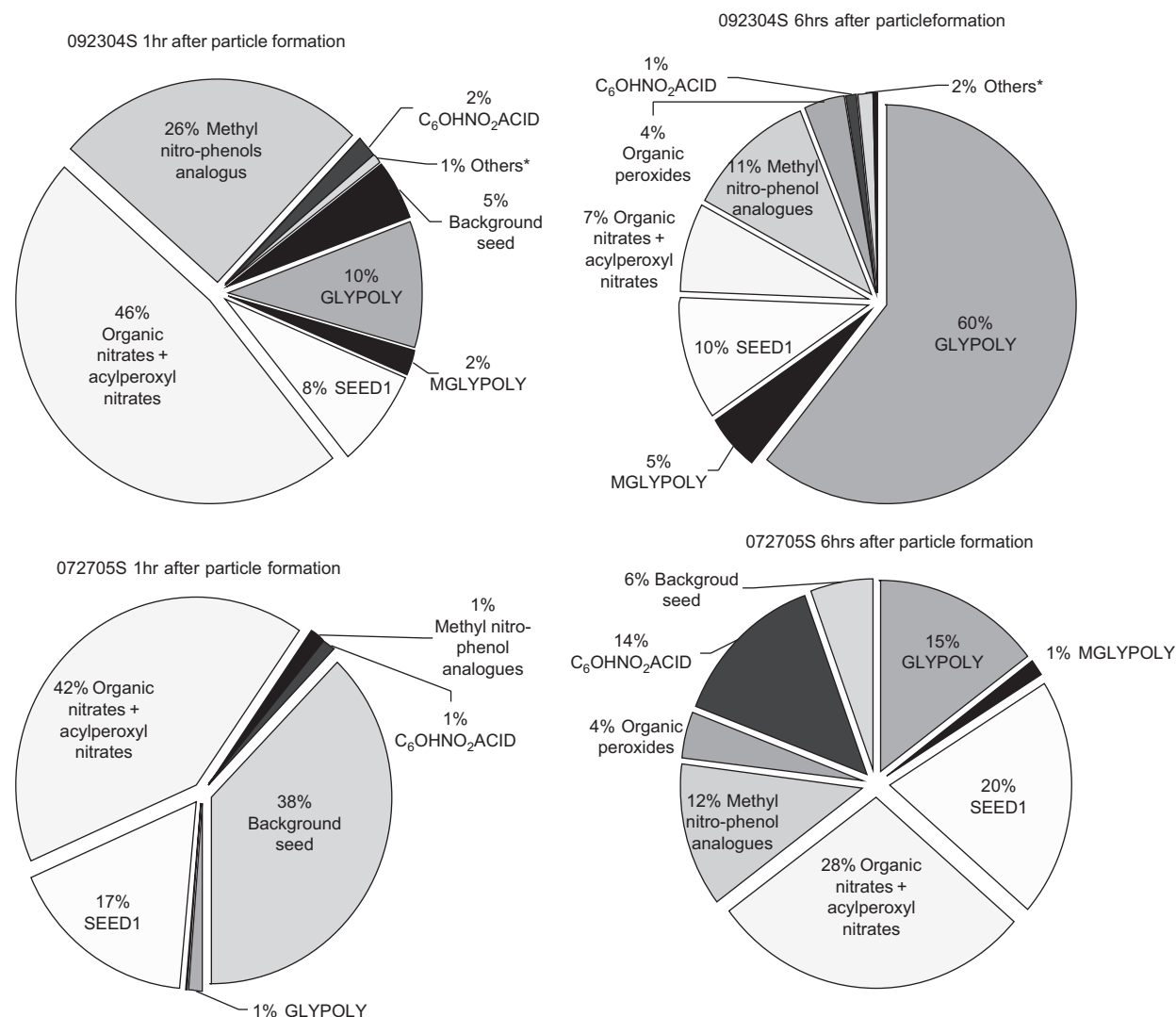[a]The species' name in the mechanism.

Fig. 5. Evolution of aerosol composition (% of mass) with time under different initial reactant concentrations. Species names correspond to structures in Table 2. *Others means the sum of all other partitioning species not listed in Table 2.

products vary depending on initial experimental conditions. Offenberg et al. (2006) showed that the heat of vaporization, $\Delta H_{\mathrm{vap,eff}}^{25-300}$, for SOA formed in the photo-oxidation of toluene at steady-state conditions (average of 6 h of reaction) in their smog chamber was similar to that formed from nebulized glyoxal. It is important to note, however, that the relative amount of different SOA species dramatically changes with time (Fig. 5). For example, in the 092304S experiment of this study, which started with 0.980 ppm V toluene and 0.280 ppm NO, the mass fraction of GLYPOLY in the aerosol phase was 10% at the time particle growth begins and it increased to 61% at the end of the experiment.

The mass fraction of total organic nitrates and acylperoxy nitrates was as high as 47% when particles started growing and it decreased to 7% at the end of the experiment. At the maximum aerosol concentration, the oligomers formed from glyoxal, methyl glyoxal and C14KETENE contributed 75% of the total particle mass, while organic nitrates, acylperoxy nitrates and methyl nitrophenol analogues accounted for the other 18%.

The speciation of simulated toluene aerosol also changes with the initial toluene concentration and the initial concentration ratio of toluene to NO (Fig. 5). In general, with decreasing toluene/NO ratios, the relative amount of total organic nitrates
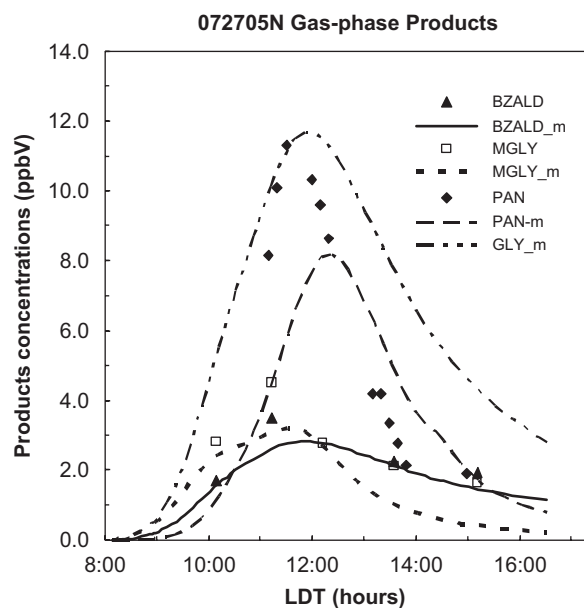
072705N Gas-phase Products

Fig. 6. Simulation (lines) vs. data (symbols) of gas-phase PAN benzaldehyde, glyoxal and methyl glyoxal.

and acylperoxy nitrates in the particle phase increases, and the mass fraction of total oligomers and organic peroxides decreases. This is because with decreasing toluene/NO ratios, relatively more NO is present in the system and more RO_2 radicals will react with NO and less will react with HO_2 and other RO_2 radicals. Hence, more organic nitrates and less organic peroxides are formed in the system. For the low toluene concentrations experiment, 072705S, the most abundant particle-phase species at the end of the experiment are organic nitrates which account for 27% of the total aerosol mass. They are followed by SEED1 that contributes 20% of the mass, GLYPOLY 17%, methyl nitro-phenol analogues 13% and C6OHNO2ACID 13%. C6OH-NO2ACID is a degradation product of cresol, and it accounts for significant aerosol mass only in the low-concentration systems.

Model simulations of gas-phase products are shown in Fig. 6. The model tracks measured gas-phase benzaldehyde. It also reasonably simulates the methyl glyoxal time concentration profile, although it tends to under-predict the maximum methyl glyoxal concentration by 29%. The model reasonably fits PAN formation, although model simulation is a little bit slower than the experimental data. When the UNC toluene mechanism is used to simulate the "mid-NO_x" toluene experimental data

obtained from the European Photoreactor (EU-PHORE), our model tracks well the timing of glyoxal formation and underestimates the maximum glyoxal concentration by ~25% (Hu and Kamens, 2007).

In summary, the mechanism presented in this paper simulates aerosol formation from the atmospheric oxidation of toluene in the presence of NO_x and natural sunlight. It does this over a range of temperatures, concentrations and toluene to NO ratios. In a companion paper (Hu and Kamens, 2007), we explore some of the uncertainties associated with the mechanism and evaluate its performance against experimental data generated by other research groups.

Acknowledgments

Appendix A. Supplementary materials

Supplementary data associated with this article can be found in the online version at doi:10.1016/j.atmosenv.2007.04.025.

References

Bahreini, R., Keywood, M.D., Ng, N.L., Varutbangkul, V., Gas, S., Flagan, R.C., Seinfeld, J.H., Worsnop, D.R., Jimenez, J.L., 2005. Measurements of secondary organic aerosol from oxidation of cycloalkenes, terpenes, and *m*-xylene using an aerodyne aerosol mass spectrometer. Environmental Science and Technology 39 (15), 5674–5688.

Barnes, I., Klotz, B., Becker, K.H., 1996. Aromatic hydrocarbon oxidation mechanisms: new developments. In: Air & Waste Management Association 89th Annual Meeting & Exhibition, Nashville, Tennessee.

Bloss, C., Wagner, V., Jenkin, M.E., Volkamer, R., Bloss, W.J., Lee, J.D., Heard, D.E., Wirtz, K., Martin-Reviejo, M., Rea, G., Wenger, J.C., Pilling, M.J., 2005. Development of a detailed chemical mechanism (MCMv3.1) for the atmospheric oxidation of aromatic hydrocarbons. Atmospheric Chemistry and Physics 5, 641–664.

Broyles, D.A., Carpenter, B.K., 2005. Experimental detection of one case of benzene epoxidation by a peroxy radical and

computational prediction of another. Journal of Organic Chemistry 70 (21), 8642–8644.

Calvert, J.G., Atkinson, R., Becker, K.H., Kamens, R.M., Seinfeld, J.H., Wallington, T.J., Yarwood, G., 2002. The Mechanisms of Atmospheric Oxidation of Aromatic Hydrocarbons. Oxford University Press, Inc., New York.

Carter, W.P.L., Atkinson, R., Winer, A.M., Pitts, J.N.J., 1981. Evidence for chamber-dependent radical sources: impact on kinetic computer models for air pollution. International Journal of Chemical Kinetics 13 (8), 735–740.

Dechapanya, W., Eusebi, A., Kimura, Y., Allen, D.T., 2003a. Secondary organic aerosol formation from aromatic precursors. 1. Mechanism for individual hydrocarbons. Environmental Science and Technology 37 (16), 3662–3670.

Dechapanya, W., Eusebi, A., Kimura, Y., Allen, D.T., 2003b. Secondary organic aerosol formation from aromatic precursors. 2. Mechanisms for lumped aromatic hydrocarbons. Environmental Science and Technology 37 (16), 3671–3679.

Derwent, R.G., Jenkin, M.E., Saunders, S.M., 1996. Photochemical ozone creation potentials for a large number of reactive hydrocarbons under European conditions. Atmospheric Environment 30 (2), 181–199.

Durham, L.J., Wurster Jr., C.F., Moshe, H., 1958. Peroxides. VIII. The mechanism for the thermal decomposition of *n*-butyl hydroperoxide and *n*-butyl 1-hydroxybutyl peroxide. Journal of American Chemical Society 80, 332–337.

Edney, E.O., Driscoll, D.J., Weathers, W.S., Kleindienst, T.E., Conver, T.S., McIver, C.D., Li, W., 2001. Formation of polyketones in irradiated toluene/propylene/NO$_x$/air mixtures. Aerosol Science and Technology 35 (6), 998–1008.

Ehhalt, D.H., 1999. Gas Phase Chemistry of the Troposphere. Springer, New York, pp. 21–109.

Gao, S., NG, N.A., Keywood, M., Varutbangkul, V., Bahreini, R., Nenes, A., He, J., Yoo, K.Y., Beauchamp, J.L., Hodyss, R.P., Flagan, R.C., Seinfeld, J.H., 2004. Particle phase acidity and oligomer formation in secondary organic aerosol. Environmental Science and Technology 38 (24), 6582–6589.

Glasstone, S., Laidler, K.J., Eyring, H., 1941. The Theory of Rate Processes: The Kinetics of Chemical Reactions, Viscosity, Diffusion and Electrochemical Phenomena. McGraw-Hill, New York.

Griffin, R.J., Dabdub, D., Seinfeld, J.H., 2005. Development and initial evaluation of a dynamic species-resolved model for gas phase chemistry and size-resolved gas/particle partitioning associated with secondary organic aerosol formation. Journal of Geophysical Research 110, D05304.

Grosjean, D., Fung, K., 1982. Collection efficiencies of cartridges and microimpingers for sampling of aldehydes in air as 2,4-dinitrophenylhydrzaones. Analytical Chemistry 54, 1221–1224.

Grossman, R., 1999. The Art of Writing Reasonable Organic Reaction Mechanisms. Springer, New York.

Hamilton, J.F., Webb, P.J., Lewis, A.C., Reviejo, M.M., 2005. Quantifying small molecules in secondary organic aerosol formed during the photo-oxidation of toluene with hydroxyl radicals. Atmospheric Environment 39, 7263–7275.

Ho, S.S.H., Yu, J.Z., 2004. Determination of airborne carbonyls: comparison of a thermal desorption/GC method with the standard DNPH/HPLC method. Environmental Science and Technology 38 (3), 862–870.

Holes, A., Esebi, A., Grosgean, D., Allen, D., 1995. FTIR analysis of aerosol formed in the presence of the photooxida-

tion of 1,2,4-trimethylbenzene. Aerosol Science and Technology 26, 516–526.

Hu, D., Kamens, R.M., 2007. Evaluation of the UNC toluene–SOA mechanism with respect to other chamber studies and key model parameters, Atmospheric Environment, doi:10.1016/jatmosenv.2007.04.026.

Hurley, M.D., Sololov, O., Wallington, T., Tawekawa, H., Karasawa, M., Klotz, B., Barnes, I., Becker, K.H., 2001. Organic aerosol formation during the atmospheric degradation of toluene. Environmental Science and Technology 35, 1358–1366.

Jang, M., Kamens, R.M., 1998. A thermodynamic approach for modeling partitioning of semivolatile organic compounds on atmospheric particulate matter: humidity effects. Environmental Science and Technology 32 (9), 1237–1243.

Jang, M., Kamens, R.M., 2001a. Atmospheric secondary aerosol formation by heterogeneous reactions of aldehydes in the presence of a sulfuric acid aerosol catalyst. Environmental Science and Technology 35 (24), 4758–4766.

Jang, M., Kamens, R.M., 2001b. Characterization of secondary aerosol from the photooxidation of toluene in the presence of NO$_x$ and 1-propene. Environmental Science and Technology 35 (18), 3626–3639.

Jang, M., Czoschke, N.M., Lee, S., Kamens, R.M., 2002. Heterogeneous atmospheric aerosol production by acid-catalyzed particle-phase reactions. Science (Washington, DC, United States) 298 (5594), 814–817.

Jang, M., Lee, S., Kamens, R.M., 2003. Organic aerosol growth by acid-catalyzed heterogeneous reactions of octanal in a flow reactor. Atmospheric Environment 37 (15), 2125–2138.

Jeffries, H., Kessler, M., Gery, M., 1998. MComp/MEval: the morphecule reaction mechanism compiler/solver development and testing of a new photochemical reaction mechanism.

Jeffries, H., Sexton, K., Adelman, Z., 1999. Auxiliary mechanisms (wall models) for UNC outdoor chamber. EPA/600/R-00/076.

Jenkin, M.E., Saunders, S.M., Pilling, M.J., 1997. The tropospheric degradation of volatile organic compounds: a protocol for mechanism development. Atmospheric Environment 33 (1), 81–104.

Joback, K.G., Reid, R.C., 1987. Estimation of pure-component properties from group contributions. Chemical Engineering Communication 57, 233–243.

Johnson, D., Jenkin, M.E., Wirtz, K., Martin-Reviejo, M., 2004. Simulating the formation of secondary organic aerosol from the photooxidation of toluene. Environmental Chemistry 1, 150–165.

Johnson, D., Jenkin, M.E., Wirtz, K., Martin-Reviejo, M., 2005. Simulating the formation of secondary organic aerosol from the photooxidation of aromatic hydrocarbons. Environmental Chemistry 2, 35–48.

Kalberer, M., Paulsen, D., Sax, M., Steinbacher, M., dommen, J., Prevot, A.S.H., Fisseha, R., Weingartner, E., Frankevich, V., Zenobi, R., Baltensperger, U., 2004. Identification of polymers as major components of atmospheric organic aerosols. Science 303 (5664), 1659–1662.

Kamens, R.M., Jaoui, M., 2001. Modeling aerosol formation from α-pinene + NO$_x$ in the presence of natural sunlight using gas-phase kinetics and gas–particle partitioning theory. Environmental Science and Technology 35 (7), 1394–1405.

Kamens, R., Jang, M., Chien, C.-J., Leach, K., 1999. Aerosol formation from the reaction of α-pinene and ozone using a gas-phase kinetics-aerosol partitioning model. Environmental Science and Technology 33 (9), 1430–1438.

Killus, J.P., Whitten, G.Z., 1990. Background reactivity in smog chambers. International Journal of Chemical Kinetics 22 (6), 547–575.

Kleindienst, T.E., Conver, T.S., McIver, C.D., Edney, E.O., 2004. Determination of secondary organic aerosol products from the photooxidation of toluene and their implications in ambient PM2.5. Journal of Atmospheric Chemistry 47 (1), 79–100.

Klotz, B., Barnes, I., Becker, K.H., 1999. Kinetic study of the gas-phase photolysis and OH radical reaction of E,Z- and E,E-2,4-hexadienedial. International Journal of Chemical Kinetics 31, 689–697.

Kroll, J.H., Ng, N.L., Murphy, S.M., Varutbangkul, V., Flagan, R.C., Seinfeld, J.H., 2005. Chamber studies of secondary organic aerosol growth by reactive uptake of simple carbonyl compounds. Journal of Geophysics Research 110, D23207.

Kwok, E.S.C., Atkinson, R., 1995. Estimation of hydroxyl radical reaction rate constants for gas-phase organic compounds using a structure–reactivity relationship: an update. Atmospheric Environment 29, 1685–1695.

Kwok, E.S.C., Aschmann, S.M., Atkinson, R., Arey, J., 1997. Products of the gas-phase reactions of o-, m-, and p-xylene with the OH radical in the presence and absence of NO_x. Journal of the Chemical Society, Faraday Transactions 93, 2847–2854.

Lee, S., Jang, M., Kamens, R.M., 2004. SOA formation from the photooxidataion of α-pinene in the presence of freshly emitted diesel soot exhaust. Atmospheric Environment 38, 2597–2605.

Lehtinen, C., Nevalainen, V., Brunow, G., 2001. Experimental and computational studies on solvent effects in reactions of peracid-aldehyde adducts. Tetrahedron 57 (22), 4741–4751.

Leungsakul, S., Jeffries, H.E., Kamens, R.M., 2005a. A kinetic mechanism for predicting secondary aerosol formation from the reactions of D-limonene in the presence of oxides of nitrogen and natural sunlight. Atmospheric Environment 39 (37), 7063–7082.

Leungsakul, S., Jaoui, M., Kamens, R.M., 2005b. Kinetic mechanism for predicting secondary organic aerosol formation from the reaction of D-limonene with ozone. Environmental Science and Technology 39 (24), 9583–9594.

Liggio, J., Li, S.-M., McLaren, R., 2005a. Heterogeneous reactions of glyoxal on particulate matter: identification of acetals and sulfate esters. Environmental Science and Technology 39 (6), 1532–1541.

Liggio, J., Li, S.-M., McLaren, R., 2005b. Reactive uptake of glyoxal by particulate matter. Journal of Geophysical Research 110, D10304.

Liu, X., Jeffries, H.E., Sexton, K.G., 1999. Atmospheric photochemical degradation of 1,4-unsaturated dicarbonyls. Environmental Science and Technology 33 (23), 4212–4220.

Mackay, D.B.A., Chan, D.W., Shiu, W.Y., 1982. Vapor pressure correlations for low-volatility environmental chemicals. Environmental Science and Technology 16, 645–649.

Makar, P.A., Moran, M.D., Scholtz, M.T., Taylor, A., 2003. Speciation of volatile organic compound emission for regional air quality modeling of particulate matter and ozone. Journal of Geophysical Research 108, D2,4041.

Matsumoto, M., Yasuoka, K., Kataoka, Y., 1994. Evaporation and condensation at a liquid surface. II. Methanol. The Journal of Chemical Physics 101, 7912–7917.

Nielsen, T., Platz, J., Granby, K., Hansen, A.B., Skov, H., Egelov, A.H., 1998. Particulate organic nitrates: sampling and night/day variation. Atmospheric Environment 32 (14/15), 2601–2608.

Noziere, B., Barnes, I., 1998. Evidence for formation of a PAN analog of pinonic structure and investigation of its thermal stability. Journal of Geophysical Research [Atmosphere] 103, 25587–25597.

Odum, J.R., Jungkamp, T.P.W., Griffin, R.J., Forstner, H.J.L., Flagan, R.C., Seinfeld, J.H., 1997. Aromatics, reformulated gasoline, and atmospheric organic aerosol formation. Environmental Science and Technology 31 (7), 1890–1897.

Offenberg, J.H., Kleindienst, T.E., Jaoui, M., Lewandowski, M., Edney, E.O., 2006. Thermal properties of secondary organic aerosols. Geophysical Research Letters 33, L03816.

Pankow, J.F., 1994. An absorption model of gas/particle partitioning of organic compounds in the atmosphere. Atmospheric Environment 28, 185–188.

Piccot, S.D., Watson, J.J., Jones, J.W., 1997. A global inventory of volatile organic compounds emissions from anthropogenic sources. Journal of Geophysical Research 97, 9897–9912.

Pun, B.K., Griffin, R.J., Seigneur, C., Seinfeld, J.H., 2002. Secondary organic aerosol. 2. Thermodynamic model for gas/particle partitioning of molecular constituents. Journal of Geophysical Research [Atmosphere] 107 (D17), AAC4/1–AAC4/15.

Saunders, S.M., Jenkin, M.E., Derwent, R.G., Pilling, M.J., 2003. Protocol for the development of the Master Chemical Mechanism, MCM v3 (Part A): tropospheric degradation of non-aromatic volatile organic compounds. Atmospheric Chemistry and Physics 3, 161–180.

Stein, S.E., Brown, R.L., 1994. Estimation of normal boiling points from group contributions. Journal of Chemical Information and Computer Sciences 34, 581–587.

Stroud, C.A., Makar, P.A., Michelangeli, D.V., Mozurkewich, M., Hastie, D.R., Bardu, A., Humble, J., 2004. Simulating organic aerosol formation during the photooxidation of toluene/NO_x mixtures: comparing the equilibrium and kinetic assumption. Environmental Science and Technology 38 (5), 1471–1479.

Suh, I., Zhang, R., Molina, L.T., Molina, M.J., 2003. Oxidation mechanism of aromatic peroxy and bicyclic radicals from OH-toluene reactions. Journal of American Chemical Society 125 (41), 12655–12665.

Tolocka, M.P., Jang, M., Ginter, J.M., Cox, F.J., Kamens, R.M., Johnston, M.V., 2004. Formation of oligomers in secondary organic aerosol. Environmental Science and Technology 38 (5), 1428–1434.

Voicu, I., 2003. A Revised Carbon Bond Mechanism. The University of North Carolina at Chapel Hill, Department of Environmental Sciences and Engineering.

Yasuoka, K., Matsumoto, M., Kataoka, Y., 1994. Evaporation and condensation at a liquid surface. I. Argon. The Journal of Chemical Physics 101, 7904–7911.

Yu, J., Jeffries, H.E., Sexton, K.G., 1997. Atmospheric photo-oxidation of alkylbenzenes—I. Carbonyl product analyses. Atmospheric Environment 31 (15), 2261–2280.
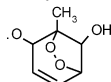
Zhao, L., Li, P., Yalkowsky, S.H., 1999. Predicting the entropy of boiling for organic compounds. Journal of Chemical Information and Computer Sciences 39, 1112–1116.

Glossary

TOLO2: a bicyclic peroxy radical formed from OH addition to toluene, such as
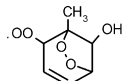
*TOLO*: a bicyclic alkoxy radical formed from OH addition to toluene, such as

C4KETALD: aldehydes with four carbon number and at least one ketone group

C5KETALD: aldehydes with five carbon number and at least one ketone group

C5OHACID: acids with five carbon number, one hydroxyl group and at least one ketone group
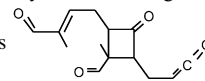
MHEXDIAL: 2-methyl-2,4-hexadienedial

C7KETENE: 2-methyl-2-butenal-4-yl-ketene
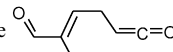
C14KETENE: a cyclobutanone derivative formed from the $2+2$ ketene-alkene cycloaddition reaction of two C7KETNENEs, which has 14 carbon numbers, one ketene group, one unsaturated carbon double bond, one cyclobutane ring and one ketone and two aldehydes groups

SEED: background aerosol that is assumed to be largely inorganic sulfates and nitrates

SEED1: nucleating product with very low vapor pressure and is considered non-volatile, that is formed from the oligomerization of C14KETENE

CH_3–*OO*: a generic peroxy radical

CH_3–*CO*–*OO*: an acyl peroxy radical

TRO_2: the sum of all alkylperoxy radicals

TSP: the sum the all particle-phase products